Int. J. Multiphase Flow Vol. 12, No. 2, pp. 149–167, 1986
Printed in Great Britain.

0301–9322/86 $3.00 + .00

STUDIES ON TWO-PHASE CROSS FLOW. PART I: FLOW CHARACTERISTICS AROUND A CYLINDER

A. INOUE, Y. KOZAWA, M. YOKOSAWA† and S. AOKI
Research Laboratory for Nuclear Reactors, Tokyo Institute of Technology, Ohokayama, Meguro-ku, Tokyo, Japan

(*Received* 12 *June* 1984; *in revised form* 29 *March* 1985)

Abstract—A two-phase flow around a body has scarcely been studied until now, though the flow is used in many industrial components. The cross flows around a spacer in a fuel assembly of light water reactors (LWR) and tube supports in a steam generator are closely related to the long-term reliability and the safety. The present study has been planned to clarify the two-phase flow and heat transfer characteristics around a body including the unknown complicated flow behavior. In the first report, the flow characteristics near and behind a cylinder which was located in a vertical upward air–water bubbly flow were investigated. From the observation of the flow patterns and the measurements of the distributions of void fraction, liquid velocity and static pressure, it is revealed that the vortex flow and the change of the static pressure and liquid velocity distributions around the cylinder resulted in the large distortion of the void fraction distribution around the cylinder. The most noticeable phenomena in the wake were that the peaks of the local void fraction appeared in the vicinity of the cylinder surface near the separation point and in the wake behind the cylinder.

1. INTRODUCTION

There are many reports dealing with a gas–liquid two-phase flow in a circular duct. In these reports, fundamental flow characteristics, i.e. void fraction, pressure drop, critical flow rate and so forth, have been revealed in detail under steady and/or unsteady state. A two-phase cross flow, however, which is very familiar in many industrial components, has been merely studied because of its heterogeneity and complexity. The reports, which we have been able to find, were Hara & Ohtani (1982) and Hulin *et al.* (1982). The former discussed the fluctuation characteristics in surface pressure, lift and drag forces on a cylinder in the two-phase cross flow. The latter reported the vortex emission behind a trapezoidal cylinder.

Recently, in nuclear power plants which are in need of the long-term integrity and the strict design bases, there exist thermal-hydraulic and safety problems concerning closely a two-phase cross flow. For example, the heat transfer rate, the critical heat flux and the subchannel mixing coefficient around fuel-rod spacers in a light water reactor (BWR & PWR) are quite different from those in the other portions in the reactor core, because the local turbulence and the void fraction around the spacers change widely. These particular flow characteristics are very important for safety designing of the reactors. Around tube supports in a steam generator of PWR, the same kind of two-phase flow with boiling plays an important role in the heat transfer characteristics. It has been experienced that the evaporation tube wall in a steam generator was thinned in the vicinity of the tube supports, so that the primary water, which was contaminated with radioactivity, leaked out in the secondary system. The cause of this accident has been reported as to be temperature fluctuations induced by flow oscillation due to an interaction of the cross flow and the structural materials.

A two-phase cross flow has scarcely been studied until now, though such flow characteristics as those in the abovementioned examples are considered to be closely related to the long-term reliability and the safety problems of the industrial components. A series of our studies, therefore, are intended to clarify the two-phase flow and heat transfer characteristics around a body, which include the unknown complicated flow behavior.

†Present address: Nuclear & Process Engineering Department, Nuclear Project Division, JGC Co., Ohokubo, Kohonan-ku, Yokohama, Kanagawa, Japan.

We have started studying on flow characteristics around a cylinder which was located in a uniform air–water bubbly flow for getting better understanding of the fundamental flow aspects, though the final objectives of our study are aimed at a steam–water two-phase flow system with heat generation from a cylinder surface.

Since local flow direction changes around a body, a two-phase cross flow is affected significantly by fluid inertia. Therefore, the quite different flow behavior between gas and liquid is induced, because of large density difference between phases. Consequently, the void fraction distribution around the body changes remarkably.

According to studies on a single-phase flow around a cylinder, Lowery & Vachon (1975) and Surry (1972), it was revealed that turbulence intensity affected the separation point, the drag coefficient and the critical Reynolds number for the transition from laminar separation to turbulent one. In a two-phase flow system it is expected that the drag coefficient and the pressure distribution around a cylinder may be different from that in a single-phase flow system, since the bubbly flow has more intensive turbulence induced by random motion of bubbles and by the wake behind bubbles than that in a single-phase flow. In a single-phase flow, moreover, the wake behind a cylinder is in unsteady state having the Kármán vortices in such wide flow condition that the Reynolds number is from scores to 10^5. The characteristics of the unsteady motion in the two-phase flow which may closely relate to the strong turbulence and the bubble behavior, are also important research subjects in a series of our studies, because those affect the heat transfer rate and the critical heat flux in case of two-phase wake flow with phase change, so that the thermal fatigue of the heat transfer tubes may be induced.

In the present study, the fundamental characteristics of the two-phase wake flow around a cylinder have been investigated in order to answer the various complicated questions as mentioned above. In the first report, we aimed at the flow behavior near and behind a cylinder which was located in a vertical upward bubbly flow. From the observation of the flow patterns and the measurements of the distributions of local void fraction, liquid velocity and static pressure, the flow characteristics in the wake around the cylinder have been discussed.

2. EXPERIMENTAL APPARATUS

The schematic of the two-phase flow loop is shown in figure 1. In the present experiment it is necessary to prepare a uniform bubbly two-phase flow corresponding to a gas flow in a wind tunnel. Namely, the bubbles having nearly the same diameter were dispersed uniformly in liquid phase and both distributions of the local void fraction and the flow velocity were uniform across the flow area which was much larger than the cross-sectional area occupied by a cylinder. The main part of the two-phase flow loop was a recirculation line constructed with large diameter pipings. Water recirculated with the jet pump in which the jet flow was produced with a high-head pump (head: 1.5 MPa, flow rate: 500 cm^3/s) located in the bypass line. The bubbly flow from the gas–liquid mixer to the separator (the total length was about 2.5 m) also induced the recirculation force as a bubble pump. The gas–liquid mixer located at about 2 m downward from the test cylinder was provided with 6 sintered metal tubes (the equivalent porous diameter was 40 μm) installed in parallel, whose outer diameter and length were 18 mm and 180 mm, respectively.

Air was injected into water through the surface of the tubes to prepare the uniform bubbly flow with uniform bubble diameters and bubble number density. Difficulty to prepare a uniform bubbly flow in a large duct was overcome by carefully setting the locations of the sintered metal tubes and independently controlling the air flow rate through each tube. Air supplied from the compressor flowed through the orifice flow meter and into the gas–liquid mixer. The bubbly flow in the test section flowed into the separator, where air was exhausted to atmosphere and water was returned again to the recirculation line. The water flow rate was measured with the calibrated pitot tube which was located in the downstream far from the jet pump.

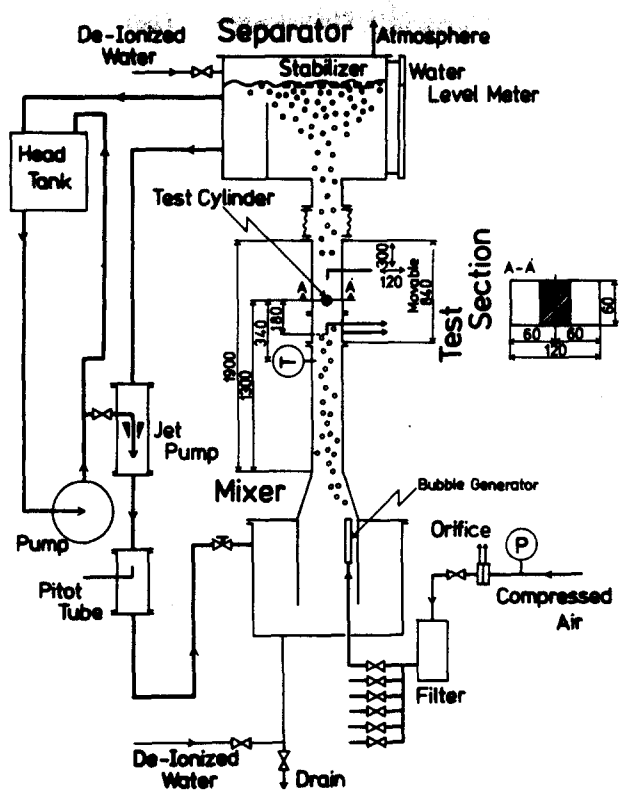

Figure 1. Schematic of two-phase flow loop.

The test section, in which the test cylinder was installed, was made of transparent plastic plates to observe the flow behavior. The cross section was a rectangle of 120 mm and 60 mm. The total length of the test section was 1900 mm and the test cylinder was installed at 1300 mm from the inlet. The bubbly two-phase flow was introduced smoothly into the test section from the mixer, via the taper duct of 300 mm length.

Figure 2 shows the vertical cross section involving the test cylinder. The cylinder length was 58 mm and its diameter was fixed on 10, 20, 30 or 40 mm. The cylinders were made of brass and their surfaces were plated with nickel. At the upstream of 180 mm from the

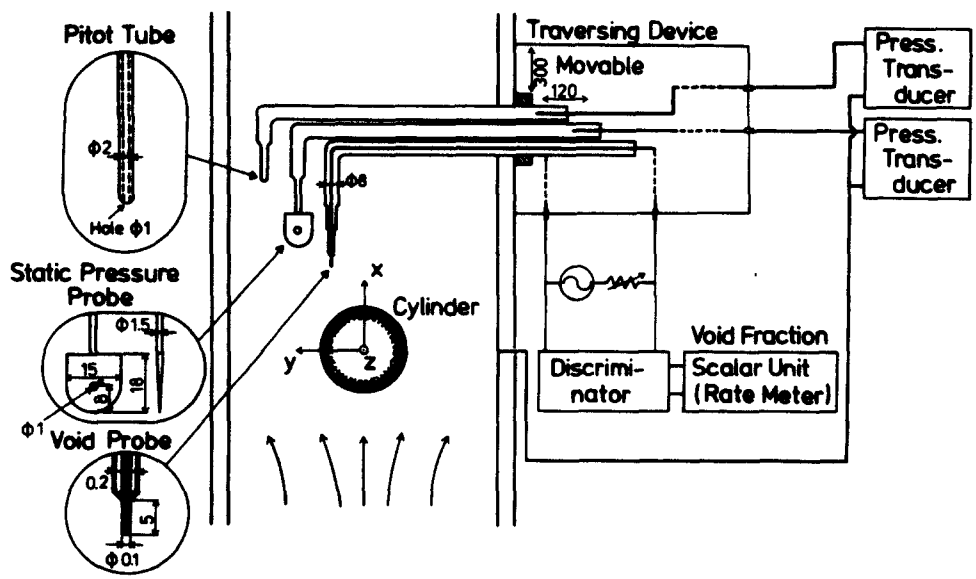

Figure 2. Vertical cross section involving test cylinder.

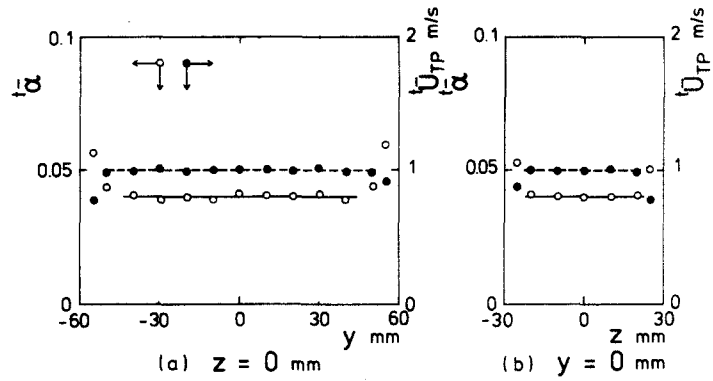

Figure 3. Examples of mean velocity distribution and void fraction distribution in main flow.

cylinder, two pairs of pitot tubes for measuring the local dynamic pressure in the main flow and needle probes for the local void fraction were installed. These instruments were supported separately at centers of a 60 mm side wall and 120 mm of one of the rectangular ducts to measure the distributions of flow velocity and void fraction in directions perpendicular to each other in the cross-sectional area of the duct. For each experimental condition, it was confirmed that the bubbly flow was uniform by using these instruments, and each flow rate through the tube in the gas–liquid mixer was adjusted to make the uniform distributions, if necessary. Examples of the mean velocity distribution and the void fraction distribution in the duct are shown in figure 3. As can be seen, the uniform distributions were realized except for the narrow regions near both duct walls.

The coordinates in the present report are shown in figure 2. The cylinder axis is z and the main flow direction is x.

3. MEASUREMENT PROCEDURES AND EXPERIMENTAL CONDITIONS

3-1. *Measurement of local void fraction*

The needle probe detecting the electrical impedance difference between contacts with air and with water was used to measure the local void fraction. The probe had a taper-shaped guide tube made of stainless steel as shown in figure 2. The outer diameters of the tube root and of the apex were 8 mm and 0.2 mm, respectively. The needle was a resin-covered stainless steel wire (0.1-mm-dia) inserted into the guide tube. The distance from the tube apex to the wire top was about 5 mm. The top of the wire was cut by using a sharp-edged knife. Thus, only the top of the wire was made electrically sensitive. In order to sharpen the cut-off signal at travelling of the air–water interface and to measure accurately the local void fraction, it is important to select a fine wire with rectangular sharp edge at the top of the wire.

The AC voltage about 2.5 V and 5 KHz was supplied between the guide tube and the wire top. The voltage change based on impedance difference between air and water was measured at an arbitrary position in the bubble flow duct. The magnitude of the voltage change was not affected by the probe position because the distance between two electrodes was always kept constant. The measurement circuit consisted of the AC source, the discriminator and the scalar unit. Both signals of water and air were distinguished by the discriminator and were transmitted to the scalar unit. The local time-averaged void fraction $'\bar{\alpha}$ was calculated with ratio of the total time occupied by air signals to the measuring time (about 1 min.).

The distributions of the local void fraction and of liquid velocity near the cylinder and in the wake behind the cylinder are to be distorted from the uniform distributions in the upstream bubbly flow of the cylinder. The wake region behind the cylinder is to spread widely in the downstream. The two-dimensional traversing device, with 0.1 mm accuracy in

the area of the 300 mm downstream from the cylinder and the duct width on the x–y plane, was used to measure local values of flow characteristics in the wake. The sensors installed on the traversing device were not only the needle probe, but also the pitot tube and the static pressure probe as described in a later section.

3.2 *Measurement of local mean velocity*

The pitot tube as shown in figure 2 was used to measure the mean velocity distribution near the cylinder and in the wake. The difference of pressure between total and reference pressure was measured with a reluctance-type pressure transducer with the accuracy ±5 Pa. The reference pressure was chosen as the pressure on the duct wall at the elevation of the center axis of the test cylinder. The dynamic pressure Δp was obtained after subtracting the static pressure from the total pressure. The measurement of the static pressure is explained in the next section 3.3. To calculate the local two-phase-averaged velocity which is nearly equal to the local liquid velocity, the dynamic pressure has to be corrected with the local void fraction at the same measuring position. This corrective method has been discussed in several literatures, Shires & Riley (1966) and Zigami *et al.* (1974). In the present experiment the correction was performed with the following equation derived by the Bernoulli's equation in a two-phase flow.

$$'\overline{U}_{TP} = \{2\Delta p/[\rho_L(1 - '\overline{\alpha}) + \rho_G '\overline{\alpha}]\}^{1/2}, \qquad [1]$$

where $'\overline{U}_{TP}$ is time- and two-phase-averaged velocity which we call "local mean velocity." Δp and $'\overline{\alpha}$ are the dynamic pressure and the time-averaged void fraction at the same position. ρ_L and ρ_G are densities of liquid- and gas-phase, respectively.

When a pitot tube is used in a two-phase flow system, it is necessary to avoid the bubbles flowing into the conduit for the pressure measurement. To do so, the volume changes of the conduit and of the sensor cell have to be made little as well as possible. The reluctance-type pressure transducer used in the present experiment satisfied these requirements. In the experiment, moreover, to remove bubbles from the conduit, water was poured on half of the conduit and flowed together with the bubbles toward the test section. After the flow rate of the poured water was gradually reduced down to zero, the pressure was measured in equilibrium state.

For the measurement in the wake behind the cylinder, the pitot tube was always oriented in parallel to the main flow direction. As the direction of $'\overline{U}_{TP}$ changed with the position near the cylinder, the local mean velocity obtained by the measurement was not the absolute value of $'\overline{U}_{TP}$ but the component of the main flow direction $'\overline{u}_{TP}$. In single-phase steady flow, when the ratio of the outer diameter to the inner one of the pitot tube is 0.5 as shown in figure 2, the velocity component of the direction of the pitot tube axis is measured slightly larger than the actual value. If the inclination angle between the local flow direction and the pitot tube axis is smaller than 25°, it is measured within errors +3% (Pankhurst & Holder 1952). Just behind the cylinder, however, the fluctuation of the local flow direction induced by the Kármán vortex is strong and it is feasible that the inclination angle becomes larger than 25°. Therefore, larger errors are conjectured there.

3.3 *Measurement of local static pressure*

It is very important to know the static pressure distribution around the cyclinder for the distribution of the void fraction, since the buoyancy force acting on the bubbles is evaluated by a product of the bubble volume and the static pressure gradient. The wake flow around the cylinder has a velocity component of the azimuthal direction. In the $x - y$ plane at the center of the cylinder axis, the flow is considered to be two dimensional. The local static pressure can be measured eliminating the dynamic pressure component by using a static

pressure probe whose pressure mouth is faced in the plane in parallel to the two-dimensional flow. The plate-shaped static pressure probe as shown in figure 2 was used after the calibration in a uniform single-phase flow. The reference pressure for the local static pressure was chosen as the pressure on the duct wall at the elevation of the center axis of the test cylinder.

For comparison with the results under various fluid velocity conditions, the static pressure coefficient Cp_{TP} obtained from the following equation was employed.

$$Cp_{TP} = (p - p_\infty)/\Delta p_0, \qquad [2]$$

where p is the static pressure and p_∞ is that in the case without the test cylinder. Δp_0 is the dynamic pressure averaged over cross-sectional area of the flow duct at the upstream of 180 mm from the cylinder.

3.4 *Experimental conditions*

The experimental conditions in the present report are tabulated as follows:

Dimension of the two-phase flow duct		120 × 60 mm
Diameter of the test cylinder	d	10, 20, 30, and 40 mm
Diameter of bubbles		3 ~ 5 mm
Mean diameter of bubbles	d_b	about 4 mm
Mean void fraction in the main flow	$\bar{\alpha}_0$	0–0.24
Mean velocity in the mean flow	$\bar{U}_{0.TP}$	0.25–2.1 m/s
Reynolds number of the two-phase flow	Re_{TP}	5×10^3–8×10^4,

where mean void fraction in the main flow $\bar{\alpha}_0$ is $\bar{\alpha}$ averaged over the cross-sectional area of the flow duct upstream of 180 mm from the cylinder. $\bar{U}_{0.TP}$ and Re_{TP} are given as follows:

$$\bar{U}_{0.TP} = \{2\Delta p_0/[\rho_L(1 - \bar{\alpha}_0) + \rho_G\bar{\alpha}_0]\}^{1/2} \qquad [3]$$

$$\mathrm{Re}_{TP} = \bar{U}_{0.TP}d/\nu_L. \qquad [4]$$

As shown in [4], the dynamic viscosity of liquid phase ν_L was used in the definition of Re_{TP} because the liquid layer which was several times as thick as the boundary layer always veiled the cylinder surface.

4. EXPERIMENTAL RESULTS

4.1 *Observation of flow pattern with photographs*

The photographs of the wake around the cylinder with 40 mm diameter are shown in figure 4. The three photographs were taken under the different mean velocity $\bar{U}_{0.TP}$, but under almost the same mean void fraction ($\bar{\alpha}_0 = 0.081 \sim 0.083$) in the upstream of the cylinder. As can be seen, the two-phase flow in the upstream of the cylinder had almost uniform distribution of bubble number density. Near both sides of the cylinder, the bubble number density increased a little, and in the downstream of the cylinder there appeared the region with high bubble number density, that is, the high void fraction region. The region occupied in the downstream of about 10 times of the cylinder diameter, but the bubble number density in the far downstream became finally uniform due to diffusion of the bubbles in the region. The number density in the region increased with mean velocity $\bar{U}_{0.TP}$. In the rear of the cylinder, there existed a liquid-rich layer with few bubbles. The thickness of the liquid layer was thicker at lower $\bar{U}_{0.TP}$. However, as $\bar{U}_{0.TP}$ increased, the high void fraction region in the downstream of the cylinder approached the cylinder and the liquid layer

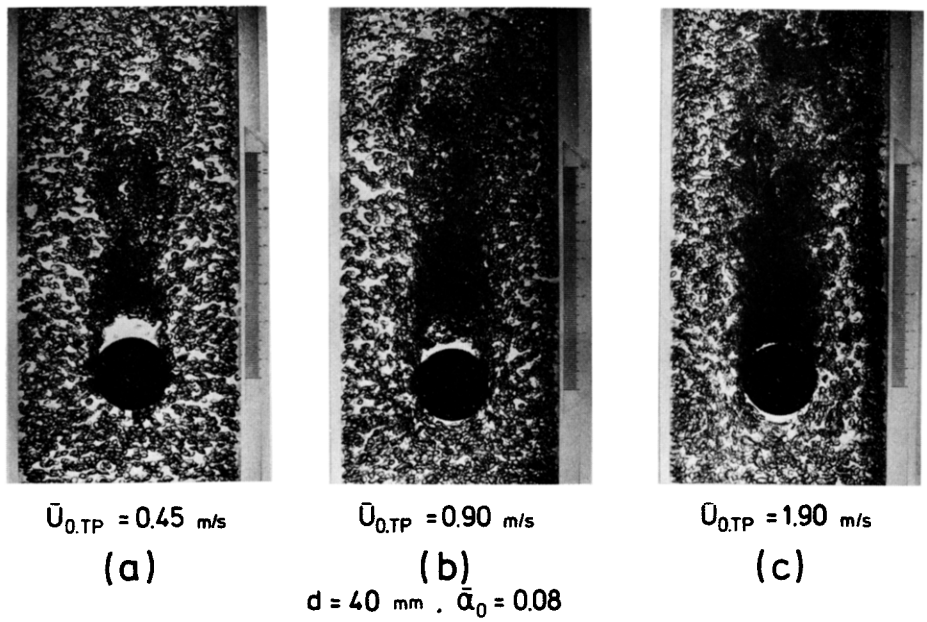

Figure 4. Photographs of wake around a cylinder.

thickness became thin. In the wake behind the cylinder, vortices formed and stagnated in some conditions. A reverse flow was produced in some region of the wake. The scale of the reverse flow was extended with the increase of $\bar{U}_{0.TP}$. In the vicinity of the rear part of the cylinder, the reverse flow rate decelerated due to the wall effect and became zero velocity on the cylinder surface. Thus, the bubbles can not invade in the rear of the cylinder and the liquid-rich layer may be produced in a balance of the flow reversal and the moving of bubbles by buoyancy force.

In the front of the cylinder, there also existed the liquid layer containing few bubbles, but thickness of the liquid layer increased with $\bar{U}_{0.TP}$, in contrast with one in the rear of cylinder. The abovementioned trend was also observed under the conditions of different $\bar{\alpha}_0$.

The flow patterns obtained in cases of d = 20 an 10 mm are shown in figures 5 and 6. In

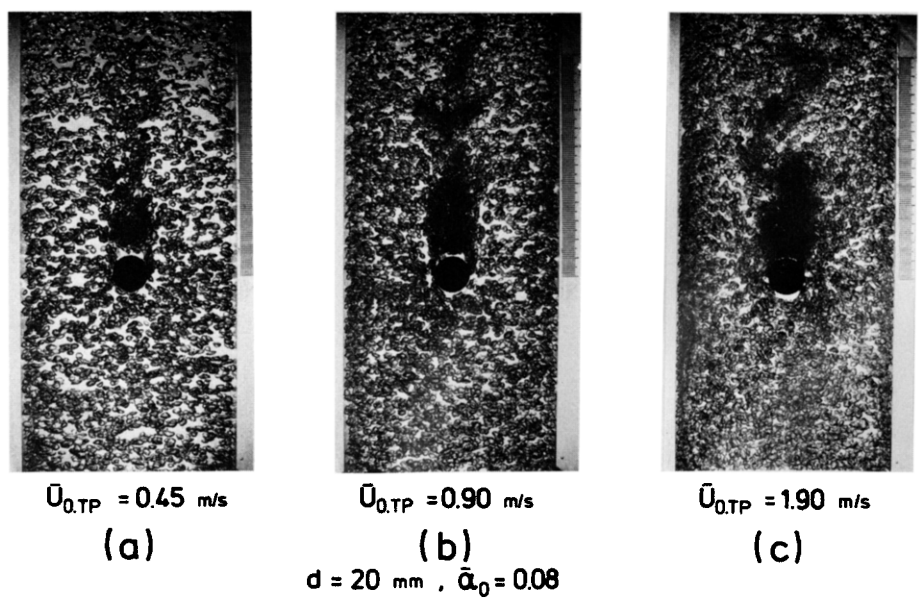

Figure 5. Photographs of wake around a cylinder.

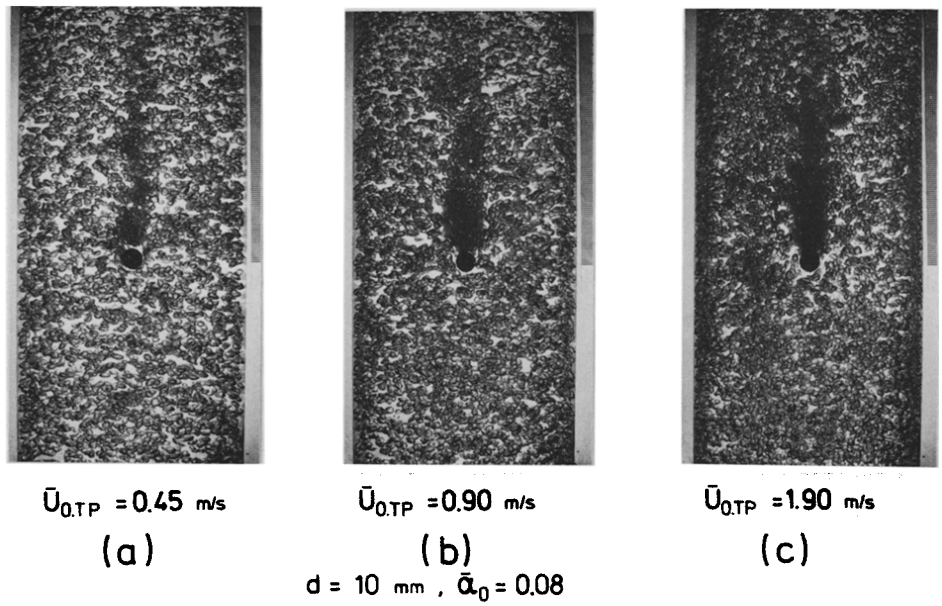

Figure 6. Photographs of wake around a cylinder.

these cases the densification of bubbles in the high void fraction region in the downstream of the cylinder was weaker than that in case of larger cylinder diameter. As shown in the case of $d = 20$ mm, the bubble number density exhibited rare and dense in the wake under certain flow conditions. The fluctuating components corresponds to the Kármán vortices in a single-phase flow observed in the wide range of the Reynolds number.

In the following sections in the present report the flow characteristics concerning the steady flow are discussed.

4.2 *Void fraction distribution*

The two-dimensional distributions of void fraction were measured in the wake behind the cylinder under several flow conditions. The void fraction distribution in the wake is significant not only to search the flow behavior but also to consider the thermal characteristics such as heat transfer rate and dryout.

The void fraction distribution in the case of $d = 40$ mm is shown in figure 7, where the mean void fractions averaged in the cross section of the duct are the same but the mean velocity of the two-phase main flow are different one another. Under the low velocity of the case (a) the local void fraction near the separation point increased up to 4 or 5 times of the mean void fraction in the main flow. This high void fraction region was elongated to the wake along the separation flow line. When the main flow velocity increased, a pair of the other high void fraction region appeared on the symmetrical positions for the $x - z$ plane. The peak value in the high void fraction region near the separation point was merely affected by the flow velocity, while the peak value in the wake increased with the flow velocity and the peak positions approached to the cylinder. Figure 8 illustrates the effect of $\bar{\alpha}_0$ on the void fraction distribution, where $\bar{U}_{0.TP}$ is constant. When $\bar{\alpha}_0$ increased in the range from 0.04 to 0.15, the peak position of the high void fraction region in the wake moved little to the downstream and the void fraction distribution did not greatly change. In a bubbly two-phase flow $\bar{\alpha}_0$ did not greatly affect the wake flow pattern. This trend, however, has a possibility of changing in the case of $d = 40$ mm under much lower $\bar{\alpha}_0$ condition (less than 0.04) and in the case of a smaller cylinder diameter.

Figure 9 shows the effect of the cylinder diameter on the void fraction distribution, where the main flow conditions are constant. The Reynolds numbers based on the cylinder

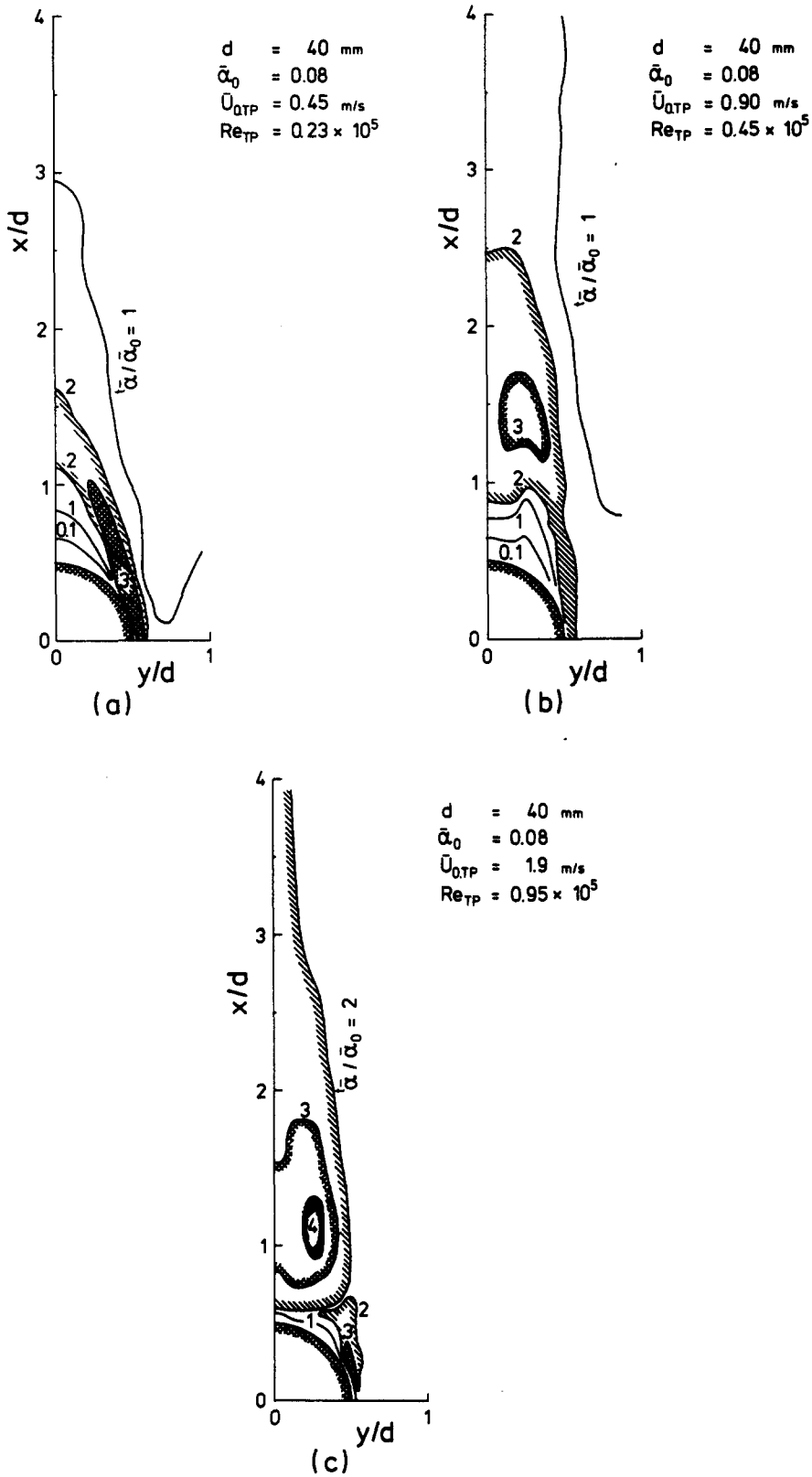

Figure 7. Effect of mean velocity in main flow $\overline{U}_{0.TP}$ on void fraction distribution (d = 40 mm, $\overline{\alpha}_0$ = 0.08).

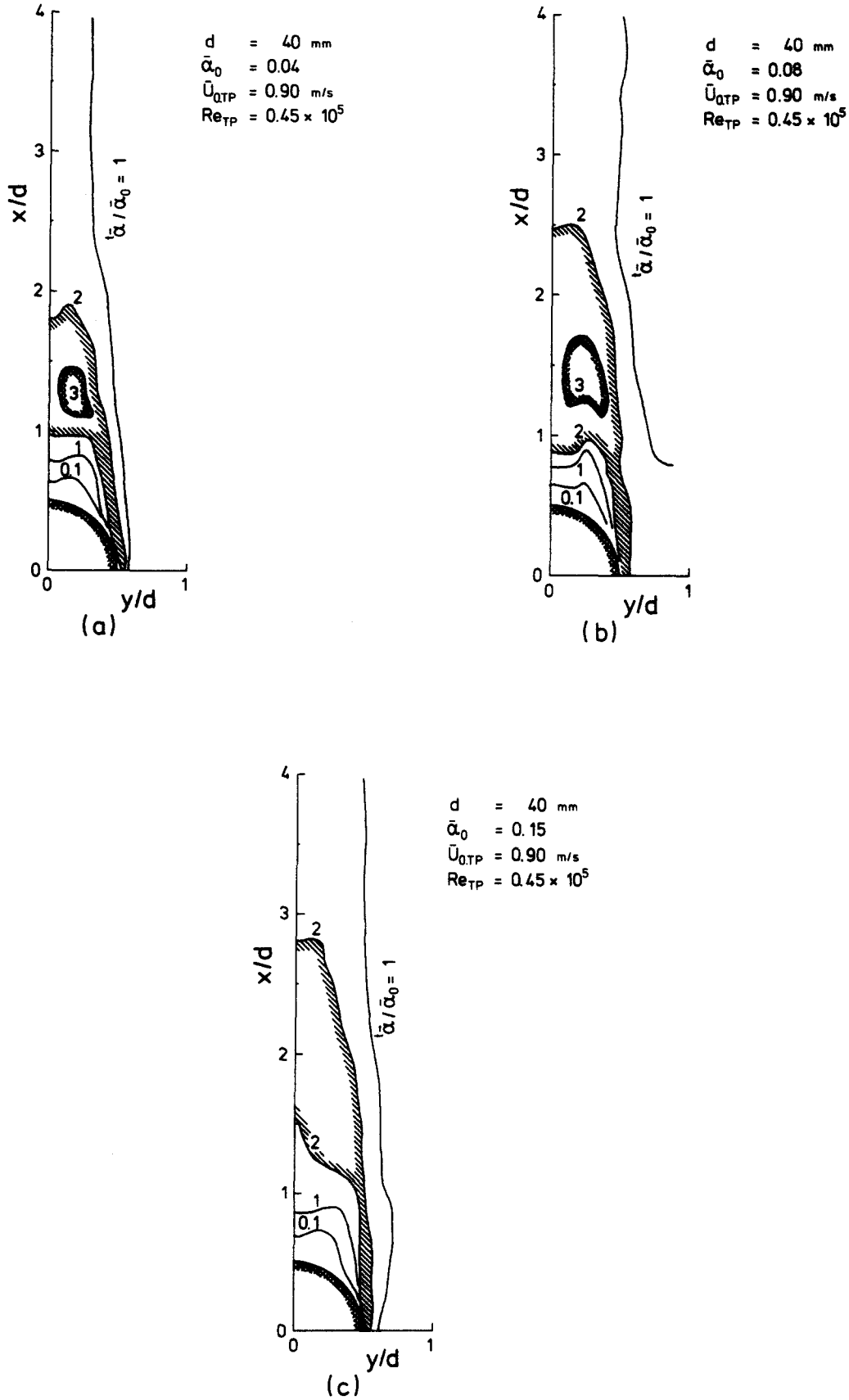

Figure 8. Effect of mean void fraction in main flow $\bar{\alpha}_0$ on void fraction distribution (d = 40 mm, $\bar{U}_{0TP}$ = 0.9 m/s).

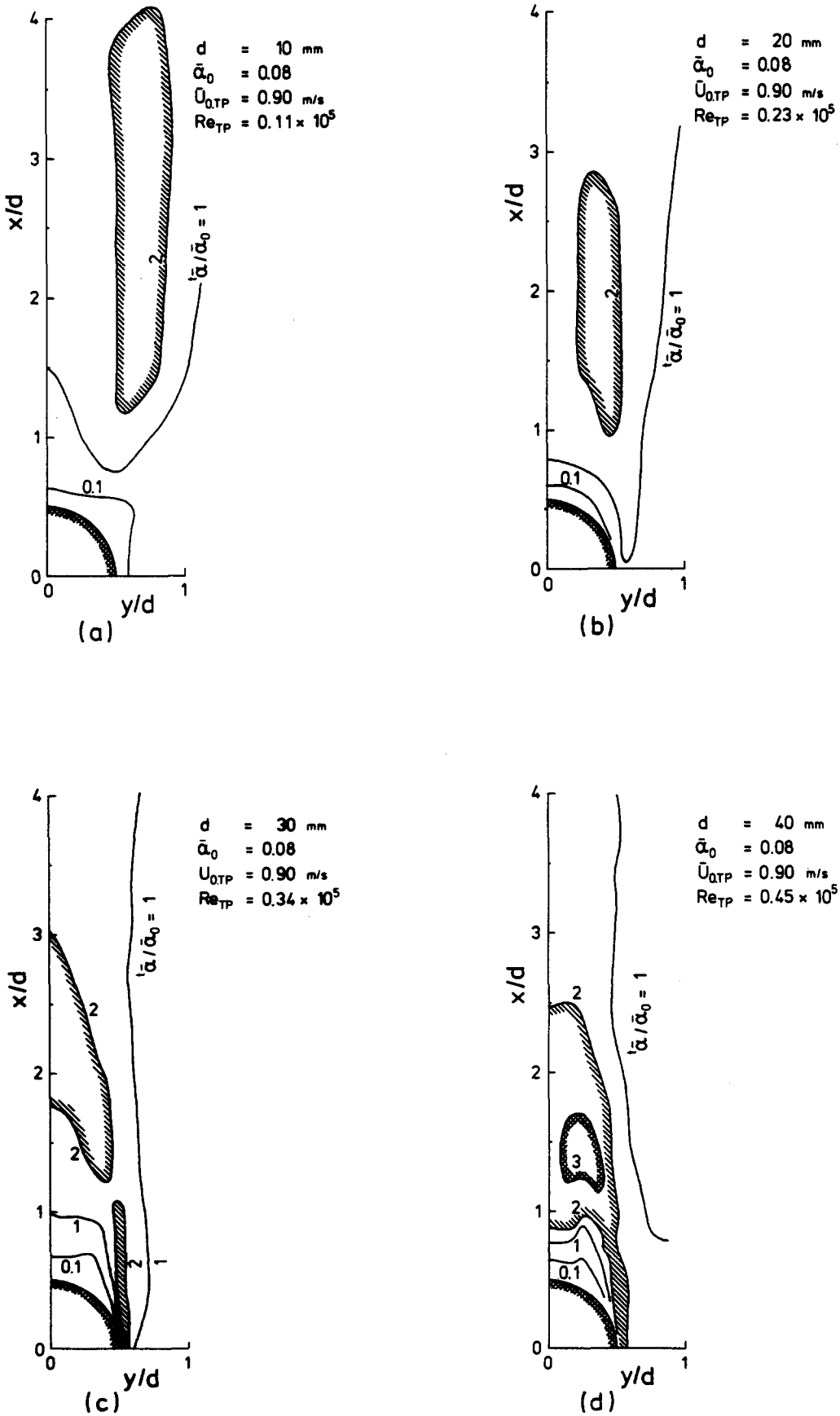

Figure 9. Effect of cylinder diameter d on void fraction distribution ($\bar{\alpha}_0$ = 0.08, $\bar{U}_{0TP}$ = 0.9 m/s).

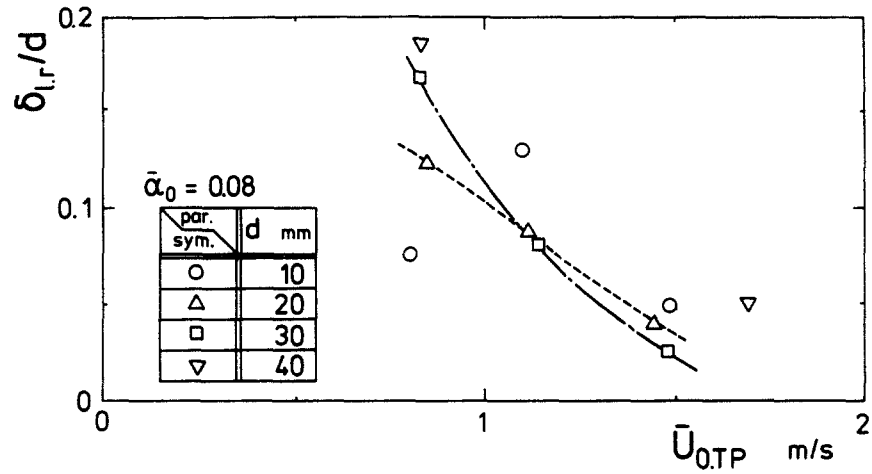

Figure 10. Liquid layer thickness on rear surface of cylinder ($\bar{\alpha}_0$ = 0.08).

diameters are different from one another, though the main flow conditions are the same. Both local void fraction peaks near the separation points and in the wake were not clear in the case of the smaller cylinder diameter, while they clearly existed in the case of large cylinder diameter. As shown in the photographs, there was only liquid layer in the rear of the cylinder, and the thickness of the layer became thinner under the higher $\overline{U}_{0.TP}$ conditions. The relation between the liquid layer thickness on the x-axis and the mean velocity in the main flow is shown in figure 10. The thickness ($\delta_{l.r}/d$) decreased almost linearly with increasing of $\overline{U}_{0.TP}$.

4.3 *Static pressure distribution*

The static pressure distribution around the cylinder were measured with the plate-shaped static pressure probe, as described in section 3.3. Since the bouyancy force acting on a bubble in a two-phase flow is equal to a product of the static pressure gradient and the bubble volume, the static pressure distribution is significant for considering the densification of the bubbles in the wake behind a cylinder. Moreover, in a two-phase flow with boiling, the phase change is affected by the static pressure distribution; that is, in low static pressure region the bubble growth rate may be accelerated, while in high static pressure region the condensation of the bubbles may occur. Consequently, the static pressure distribution is closely related to the boiling heat transfer rate and the dryout.

The local static pressure in the case without the test cylinder p_∞ is calculated with the gravitational force taking into account the mean void fraction in the two-phase main flow $\bar{\alpha}_0$ because the friction pressure loss is negligible in case of the large duct. In figures 11, 12 and 13, the static pressure distributions are illustrated by using the dimensionless pressure coefficient Cp_{TP} defined by [2]. The pressure coefficient in the figures indicates the distortion of the static pressure distribution due to the cylinder in which the gravitational pressure loss is eliminated from the measured static pressure. In the figures, moreover, distributions of Cp_{TP} in the liquid single-phase flow are compared at the same $\overline{U}_{0.TP}$ conditions. The distortion of the static pressure distribution already occurred in front of the cylinder and spread into the wake behind the cylinder. The decreasing of the local static pressure around the cylinder in the case of the two-phase flow was not so remarkable compared with that in the single-phase flow, because the turbulence in a two-phase flow is so large that the exchange of the momentum in the wake with that in the main flow occurs vigorously. The densification of bubbles in the wake behind the cylinder as shown in the void fraction distribution is interpreted by referring to the results of the pressure coefficient distribution around the cylinder. The local static pressure is obtained by adding the ($p - p_\infty$) in [2] to the water head calculated with $\bar{\alpha}_0$. The bouyancy force acting on a bubble

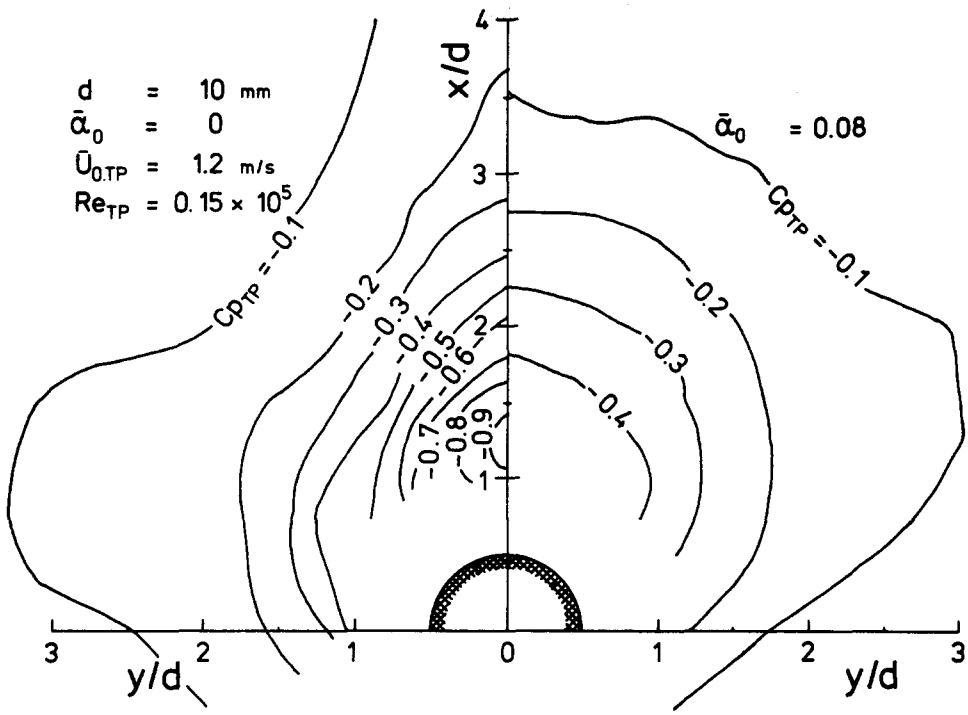

Figure 11. Static pressure distribution (d = 10 mm, $\bar{\alpha}_0$ = 0.08, $\bar{U}_{0TP}$ = 1.2 m/s).

(integration of the local static pressure on the bubble surface) is proportional to the static pressure gradient. As shown in figures 11 to 13, the pressure coefficient decreased in the direction of the surface around the cylinder. The densification of bubbles toward the cylinder occurs due to the static pressure gradient around the cylinder and the magnitude of the densification becomes larger for the larger cylinder. The stronger force acting on the bubbles

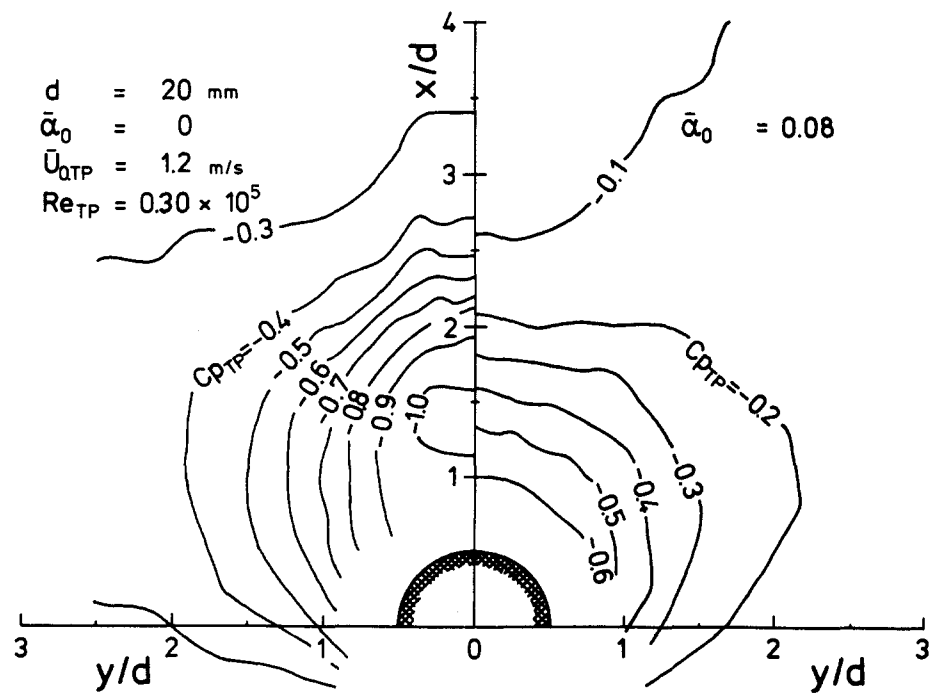

Figure 12. Static pressure distribution (d = 20 mm, $\bar{\alpha}_0$ = 0.08, $\bar{U}_{0TP}$ = 1.2 m/s).

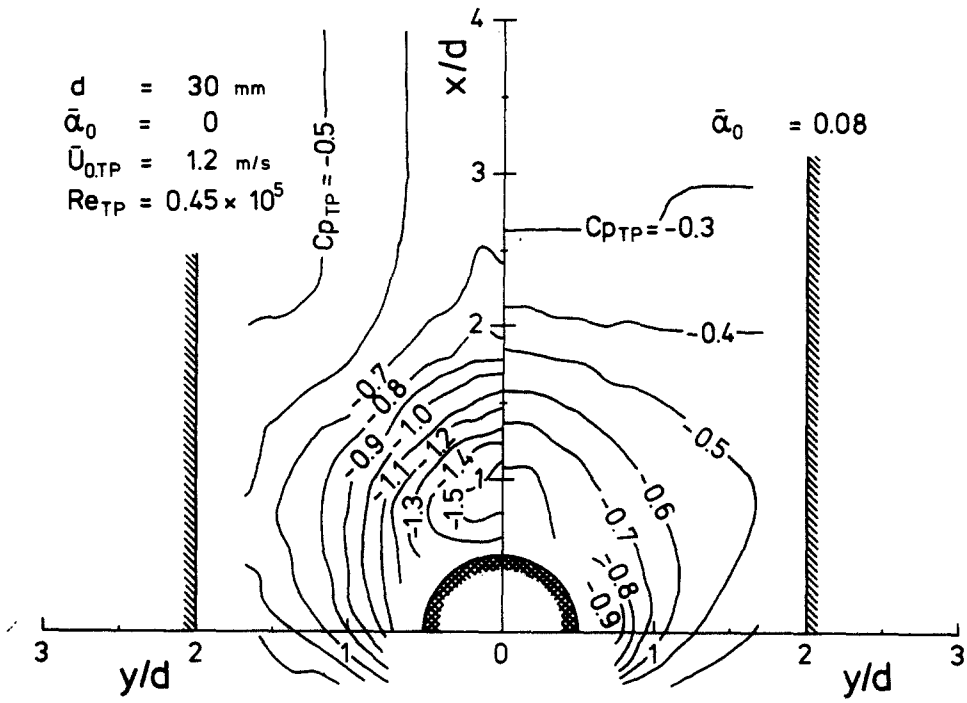

Figure 13. Static pressure distribution (d = 30 mm, $\bar{\alpha}_0$ = 0.08, $\bar{U}_{0.TP}$ = 1.2 m/s).

is induced in the case of the larger cylinder, since the gradient of Cp_{TP} toward the cylinder becomes smaller in such a case.

Figures 14 and 15 show the distribution of Cp_{TP} on the x-axis in the wake for d = 10 and 20 mm. The broken lines in the figures correspond to the real static pressure distributions which are calculated by adding the $(p - p_\infty)$ in [2] and the water head in the two-phase flow. For $x/d > 3$, the pressure coefficient Cp_{TP} based on the broken line decreased with the increase of x/d due to decrease of the water head. As can be seen in these figures, in the region of x/d = 0.5 to 1.25 the Cp_{TP} decreased and the large bouyancy force acted on the bubbles, while in the region of x/d = 1.25 to 3, the Cp_{TP} increased and the reverse buoyancy force acted on the bubbles, so that the bubbles flowed downward or were stagnant. In the wake behind the cylinder, there existed the region where the bubbles received such a strong

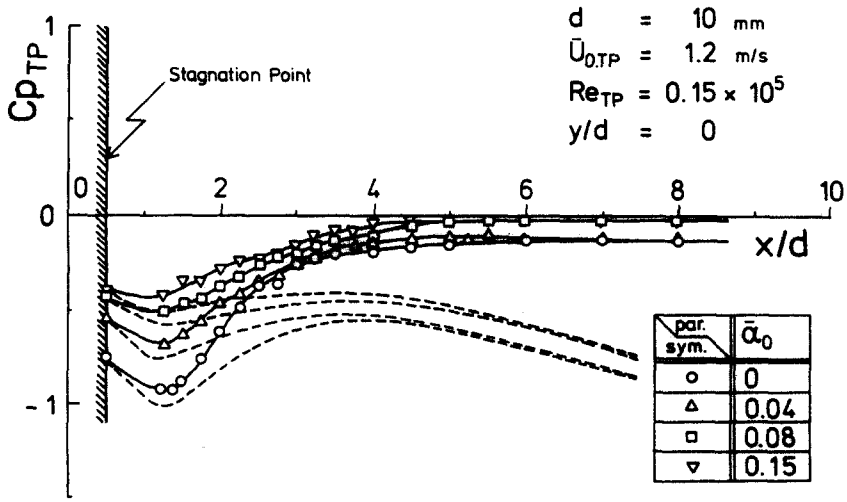

Figure 14. Distributions of static pressure on x-axis behind a cylinder (d = 10 mm, $\bar{U}_{0.TP}$ = 1.2 m/s; y/d = 0).

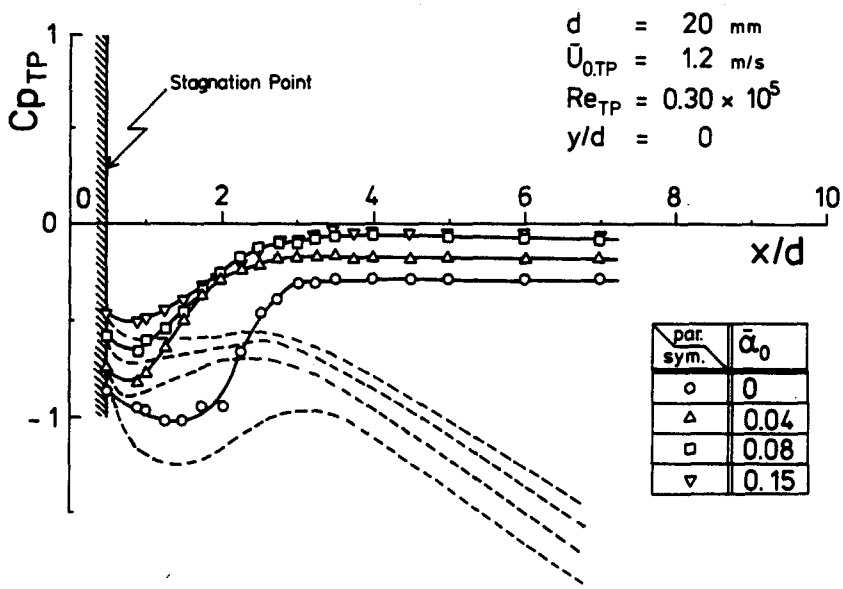

Figure 15. Distributions of static pressure on x-axis behind a cylinder (d = 20 mm, $\bar{U}_{0.TP}$ = 1.2 m/s; y/d = 0).

rising force that the bubbles could not penetrate toward the rear surface of the cylinder, and the other region, where the bubbles flowed downward or were stagnant, followed to it. The abovementioned matters are reasons why the liquid layer in the vicinity of the rear cylinder surface is produced and the peak void fraction in the wake exhibits. As shown in figures 14 and 15, when $\bar{\alpha}_0$ increased, in the region of x/d = 1.25 to 3 the gradient of Cp_{TP} decreased and then the magnitude of bubble densification became small due to an increase of the turbulence in the two-phase mixture.

4.4 *Mean velocity distribution*

The local mean velocity in the two-phase flow was obtained by using the pitot tube as described in section 3.2, where the local void fraction $'\bar{\alpha}$ was also taken into account. The static pressure tap was faced in parallel direction to the cylinder axis in order to eliminate the dynamic pressure of the azimuthal direction around the cylinder.

Figures 16, 17 and 18 show the mean velocity distributions along the main flow direction in the wakes under various cylinder diameters, where the mean void fraction in the main flow $\bar{\alpha}_0$ is 0.08. In these figures the velocity distributions in the liquid single-phase flow are compared. The increase of the local mean velocity at x/d = 0 with the cylinder diameter was caused by increasing of the flow rate due to the blockage effect of the cylinder. The local mean velocity decelerated greatly near the rear region of the cylinder (x/d = 2–4), and then recovered rapidly as flowing to the downstream and the deceleration region spread in normal direction to the main flow. The velocity recovery was more rapid than that of the single-phase flow, while the distorted region of the velocity distribution in the single-phase flow spread more widely in the normal direction than that in the two-phase flow. These two facts seem to be inconsistent, if the velocity recovery process is only affected by the intensity of turbulent diffusivity of momentum in the wake. These facts, however, are explained as follows: The turbulence scale in the wake is nearly equal to the cylinder diameter and is larger than the turbulence in a bubbly flow due to existing of the slip velocity of bubble. The intensity of turbulent diffusivity, therefore, is considered to be the same order in both single- and two-phase flow. On the other hand, the initial width of the velocity distortion region is affected by the angle of the separation point. It was observed that the separation angle seemed to shift to downstream owing to large turbulence in the boundary layer of the

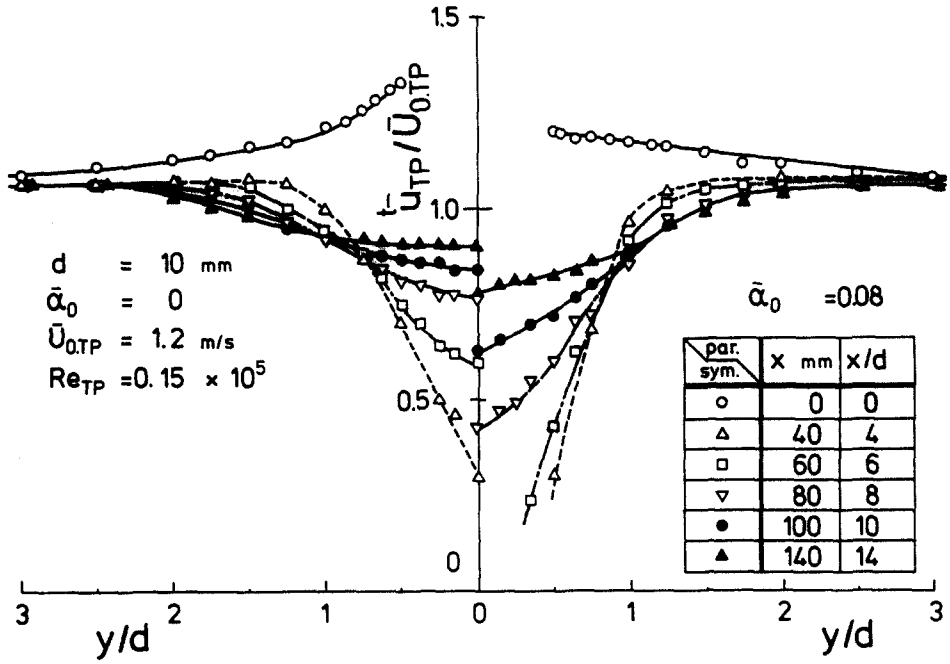

Figure 16. Recovery of mean velocity distribution in downstream of cylinder (d = 10 mm, $\bar{\alpha}_0$ = 0.08, $\bar{U}_{0.TP}$ = 1.2 m/s).

cylinder compared with that in case of a single-phase flow. The width of the wake in a two-phase flow, therefore, becomes narrower than that in a single-phase flow. The rapid velocity recovery is considered to be caused by the fact that the bubble pumping effect acts strongly in the wake due to the buoyancy force of the high void fraction region produced by the bubble densification in the wake. The void fraction distribution as described in the previous section exhibited that the bubbles in the high void fraction region diffused again in the far downstream of the wake. This bubble behavior results in inducing the liquid inflow in

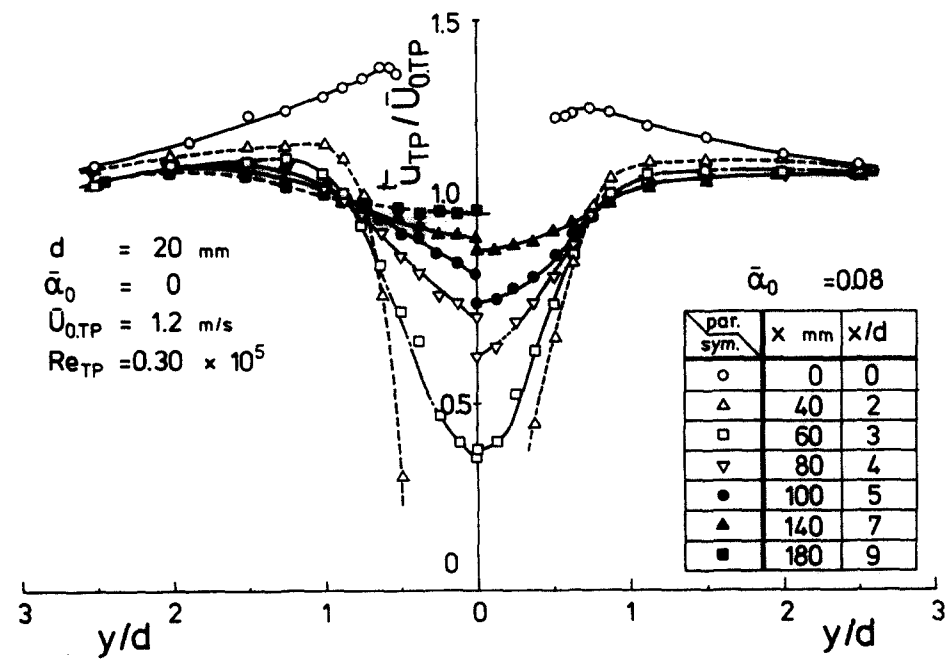

Figure 17. Recovery of mean velocity distribution in downstream of cylinder (d = 20 mm, $\bar{\alpha}_0$ = 0.08, $\bar{U}_{0.TP}$ = 1.2 m/s).

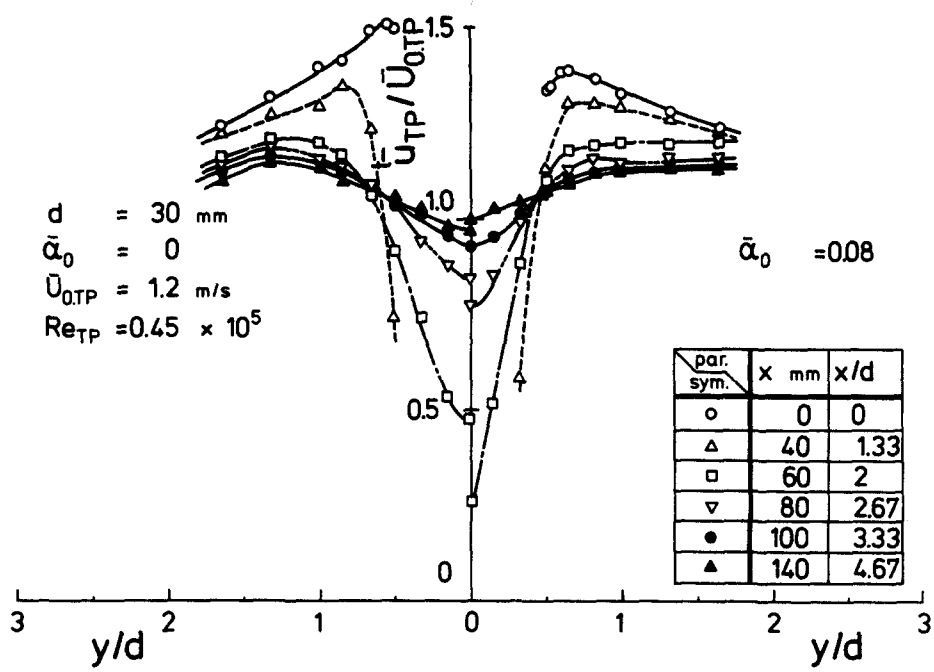

Figure 18. Recovery of mean velocity distribution in downstream of cylinder (d = 30 mm, $\bar{\alpha}_0$ = 0.08, $\bar{U}_{0.TP}$ = 1.2 m/s).

the direction to the $x - z$ plane, and the spreading of the liquid velocity distortion region is suppressed.

5. DISCUSSION

The most noticeable phenomena in the wake around a cylinder in a two-phase flow are strong bubble densification and dispersion. This bubble behavior also affects the flow characteristics. The peaks of the local void fraction (or bubble number density) appeared in the vicinity of the cylinder surface near the separation points and in the wake behind the cylinder. The causes of the bubble densification are mentioned as follows:

1. The decreasing of slip velocity ratio due to the increase of the drag coefficient of bubble;
2. The decreasing of buoyancy force on bubble due to decrease of the static pressure gradient;
3. The bubble movement in the normal direction to the main flow due to lift force induced by the liquid velocity gradient (the Magnus effect);
4. The bubble densification in the centrifugal force field due to existing of the rotational flow.

The dominant factors for increasing of the bubble drag coefficient are cited as (a) the change of turbulence in liquid phase around a bubble, (b) the coalescence of bubbles and (c) the effect of local void fraction. The first cause, however, seems to be not so significant, because in the present experimental condition the mean void fraction in the main flow is low (less than 0.24) and the turbulence in the wake behind the cylinder in a single-phase flow is more intensive than that produced in the wake behind bubbles. Causes (2), (3) and (4) become dominant in each flow field around the cylinder. For example, the liquid layer near the stagnation point in front of the cylinder becomes thick when the mean velocity in the main flow $\bar{U}_{0.TP}$ increases. The cause of this behavior is mainly in the static pressure gradient. In front of the cylinder, the static pressure increases in the direction toward the cylinder surface. The bubble can not penetrate easily in the liquid layer. The static pressure gradient

increases with the $\overline{U}_{0,TP}$, and consequently, the liquid layer thickness increases. On the other hand, in the rear of the cylinder there exists the narrow region where the static pressure increases in the direction toward the rear surface of the cylinder as shown in figures 14 and 15. The bubbles can not also penetrate in this region. In the following region behind the cylinder the static pressure decreases in the direction toward the cylinder, and the slip velocity ratio is to decrease, so that the local void fraction increases.

There exists the noticeable void fraction distribution, that is, the peak void fraction near the separation point and that in the wake behind the cylinder. In these regions the peak void fractions are produced by not only the static pressure gradient but also the lift and centrifugal forces. In the flow field near the separation point, the static pressure decreases in the direction toward the cylinder surface, so that the force which acts on bubble to move it toward the cylinder surface is produced, namely, a kind of buoyancy force. The flow near the separation point involves locally strong angular momentum induced by the interaction between the surface flow along the cylinder and the two-phase main flow. These flow characteristics are dominant causes of the densification of bubble near the separation point. In the wake behind the cylinder the reverse flow induced by the positive static pressure gradient in the x-axis interacts with the two-phase main flow, so that the strong rotational flow is also produced in the wake. The main cause of the peak void fraction in the wake is to be the centrifugal force due to the rotational flow. The static pressure distribution is shown in figures 11 to 13 and the liquid velocity distribution as shown in figures 16 to 18 produces the lift force in direction normal to the two-phase main flow. Though the mass of bubble is small, the response of the bubble movement for the various forces is not so fast due to the added mass effect. In the wake around the cylinder the bubble movement seems to be strongly affected by the static pressure gradient and the rotational flow field.

The development of the higher void fraction regions may produce severe thermal problems, namely, reduction of the heat transfer rate and/or the dryout heat flux. The peak value of the local void fraction in the wake behind the cylinder is affected so strongly by the flow characteristics that in the cross flow of rod bundle with boiling it is difficult to predict the position and the peak value of the high void fraction region unless the flow characteristics in the rod bundle will have been well known. The peak value of the void fraction near the separation point, however, is dominated by the flow behavior in the vicinity of the cylinder itself since the position of the peak is very close to the cylinder surface. The void fraction peak near the separation point has direct effect for the thermal problems. The results of the present report were obtained in the system of air–water two-phase flow without phase change. In the system of saturated steam–water two-phase flow with a heated cylinder the phenomena will be more complicated due to the additional effects of the self-vaporization and the condensation caused by static pressure change, and effect of the boiling on the solid surface. The two-phase wake flow with phase change is now under experiment.

6. CONCLUSIONS

The distributions of local void fraction, static pressure and liquid velocity in the wake around the cylinder were measured in the system of vertical upward flow of air–water uniform bubbly two-phase mixture. The rotational flow and the changes of the static pressure and mean velocity distributions around the cylinder resulted in the great distortion of the void fraction distribution near the cylinder and in the wake of the cylinder.

1. The high void fraction regions where the local void fraction was about 3 to 4 times higher than that in the two-phase main flow were produced near the separation point.
2. In the twin high-void fraction regions on the symmetrical position for the $x - z$ plane in the wake, the peak void fraction increased and the peak position came close to the cylinder as the mean velocity increased in the main flow.

3. In the front and the rear of the cylinder the liquid-rich layer where bubbles could hardly penetrate were produced owing to the static pressure gradient. The liquid layer became thicker in the front of the cylinder, and became thinner in the rear of the cylinder when the mean velocity increased.
4. The width of the wake flow region behind the cylinder in the two-phase flow was narrower than that in the liquid single-phase flow, and the recovery of the mean velocity in the wake was more rapid due to the buoyancy force on bubbles and larger turbulence in the two-phase flow.
5. The high-void fraction region produced near the separation point was so close to the cylinder that it may have greatly affected the drag force and the heat transfer characteristics, in particular, the critical heat flux.

Acknowledgements—This work has been performed by a part of the Grant-in-Aid for Scientific Research of the Ministry of Education, Science and Culture under Grant No. 342052. The authors would like to thank Mr. H. Matsuura and Mr. M. Sekiguchi (they were graduate students of the Tokyo Institute of Technology) for their assistance in conducting our experiments.

REFERENCES

HARA, F. & OHTANI, I. 1982 Vibrations of a circular cylinder in cross two-phase flow (1st report; Karmann vortex shedding and pressure fluctuations). *Trans. JSME* **C48,** 962–971.

HARA, F. 1982 Two-phase cross flow induced vibrations in a cylindrical system (2nd report, Characteristics of unsteady lift and drag forces). *Trans. JSME* (C) **48,** 1371–1379.

HULIN, J.-P., FIERFORT, C. & COUDOL, R. 1982 Experimental study of vortex emission behind bluff obstacles in a gas liquid vertical two-phase flow. *Int. J. Multiphase Flow* **8,** 475–490.

LOWERY, G. W. & VACHON, R. I. 1975 The effect of turbulence on heat transfer from heated cylinders. *Int. J. Heat Mass Transfer* **18,** 1229–1242.

PANKHURST, R. C. & HOLDER, D. W. 1952 *Wind Tunnel Technique.* Pitman.

SHIRES, G. L. & RILEY, P. J. 1966 The measurement of radial void distribution in two phase flow by isokinetic sampling. AEEW-M650, Winfrith, U. K.

SURRY, D. 1972 Some effects of intense turbulence on the aerodynamics of a circular cylinder at subcritical Reynolds number. *J. Fluid Mech.* **52,** 543–563.

ZIGAMI, T., KATAOKA, K., SERIZAWA, A. & MICHIYOSHI, I. 1974 Liquid velocity measurement in gas-liquid two-phase flow by using a pitot tube. Fall Meeting on Reactor Physics and Engineering, E-13, Atomic Energy Society of Japan.